Earth and Planetary Science Letters 563 (2021) 116882

Contents lists available at ScienceDirect

Earth and Planetary Science Letters

www.elsevier.com/locate/epsl

Asian monsoon evolution linked to Pacific temperature gradients since the Late Miocene

Jiayi Lu [a], Huan Yang [a], Michael L. Griffiths [b], Natalie J. Burls [c], Guoqiao Xiao [a], Jilong Yang [d], Jessica K. Wang [e], Kathleen R. Johnson [e], Shucheng Xie [a,*]

[a] State Key Laboratory of Biogeology and Environmental Geology, Hubei Key Laboratory of Critical Zone Evolution, School of Earth Sciences, China University of Geosciences, Wuhan 430074, China
[b] Department of Environmental Science, William Paterson University, Wayne, NJ 07470, USA
[c] Department of Atmospheric, Oceanic, & Earth Sciences, Center for Ocean-Land-Atmosphere Studies, George Mason University, Fairfax, VA 22030, USA
[d] Tianjin Center of China Geological Survey, Tianjin 300170, China
[e] Department of Earth System Science, University of California, Irvine, CA 92697, USA

ARTICLE INFO

Article history:
Received 13 September 2020
Received in revised form 3 March 2021
Accepted 6 March 2021
Available online 22 March 2021
Editor: Y. Asmerom

Keywords:
paleohydrology
Pliocene
microbial biomarkers
Asian monsoon
climate model

ABSTRACT

Considerable uncertainty remains over the nature and causes(s) of East Asian monsoon evolution since the Late Miocene, a significantly warmer period characterized by substantially weaker meridional and zonal Pacific sea surface temperature (SST) gradients than today and therefore regarded as a potential analog for current and future global warming. However, the extent to which these temperature gradients impacted rainfall patterns across East Asia, and particularly the northern extent of the monsoon domain, remains controversial. Here we present the first hydrological record extending back eight million years (Ma) for North China Plain derived from organic biomarkers preserved in a terrestrial sediment sequence. Our record shows a significant increase in monsoon rainfall during the Early Pliocene (~4.2-4.5 Ma), coincident with strengthening of Pacific meridional and zonal SST gradients, and the eastern equatorial Pacific cold tongue. This marked intensification of the monsoon rainfall in northern China is also observed in paleoclimate archives from southern Asia, but anti-phased with those from central-eastern China (including southern China), indicating a 'tripole-like' rainfall pattern over East Asia. Through a set of climate model experiments, we show that this redistribution of monsoon rainfall across East Asia during the Early Pliocene (5.33-3.6 Ma) was likely due to an equatorward contraction of the western Pacific warm pool, reduced summer convection in the western subtropical Pacific, and the strengthening of the Hadley and Walker circulations. Our study thus highlights the strong influence of Pacific Ocean temperature gradients on East Asian hydroclimate.

1. Introduction

Earth's climate underwent significant climatic changes during the late Cenozoic, particularly the Pliocene Epoch (5.33-2.58 Ma), when the Earth transitioned from relatively warm conditions to a substantially cooler climate, which was characterized by the initiation of Northern Hemisphere glaciation and the subsequent intensification of glacial-interglacial cycles during the Pleistocene (so-called "Icehouse Earth") (Fedorov et al., 2013; Wara et al., 2005). Around the same time, the climate of East Asia shifted into a state that more closely resembles today, where the genesis (or amplification) of the monsoon led to the development of the well-vegetated humid and semi-humid regions of northern China (An et al., 2014). The uplift of the Tibetan Plateau ~3.6 million years ago (Ma) (An et al., 2001) and global cooling since the early Pliocene (Wang et al., 2019) are two favored hypotheses to explain the overall strengthening of the East Asian Summer Monsoon (EASM) around this time. The orogenic mechanism has also been applied to regions affected by the westerlies, such as the aridification of Interior Asia (Guo, 2004). These hypotheses, however, remain controversial, in large part because most investigations on the late Cenozoic evolution of the EASM have focused primarily on the semi-humid region (e.g., the Chinese Loess Plateau), with a notable absence of any long-term records (e.g., Pliocene) from the humid terrestrial region of eastern China.

Annual rainfall variability across East Asia is dominated by the EASM, which is responsible for delivering seasonal moisture to the region sourced from the western Pacific and Indian Ocean, and in-

* Corresponding author.
E-mail address: xiecug@163.com (S. Xie).

https://doi.org/10.1016/j.epsl.2021.116882
0012-821X/

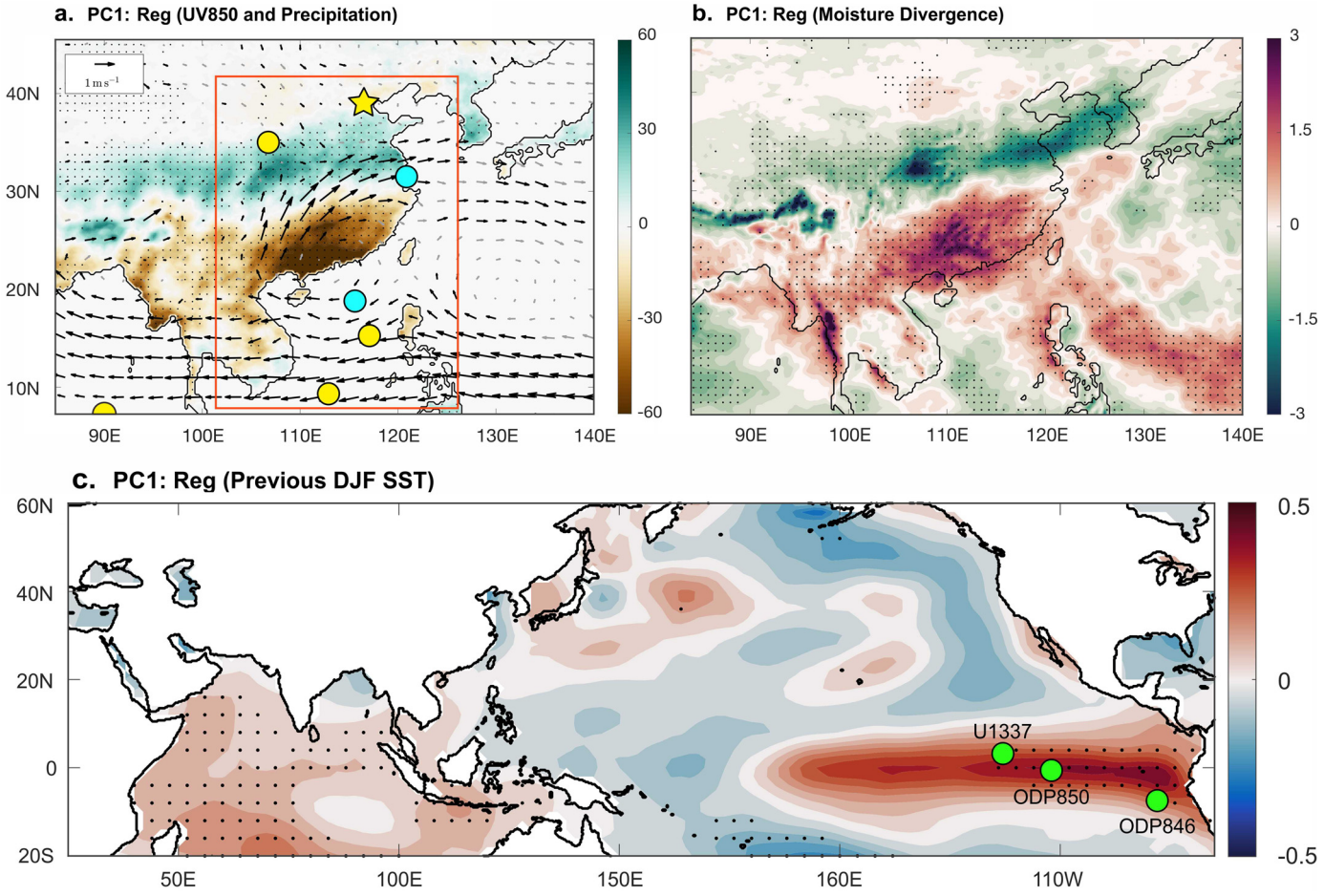

Fig. 1. Influence of ENSO on modern East Asian summer monsoon variability. **a**-**b**. Regression maps of East Asian July-August **a**, precipitation (mm, shading; PERSIANN-CDR: Ashouri et al., 2015) and 850-hPa winds ($m\,s^{-1}$, vectors; ECMWF ERA5), and **b**, vertically integrated moisture divergence (kg m^{-2}; ECMWF ERA5) onto Principal Component 1 (PC1) of precipitation. PC1 was generated from an EOF analysis of precipitation for East Asia [red box in **a** (100-124° E, 8-45° N); Fig. S1]. Symbols in **a** indicate our study site (star), along with other records from the Chinese Loess Plateau (Sun et al., 2006), Yangtze River Delta(Zhang et al., 2013), northern South China Sea (Wan et al., 2007), central (Gai et al., 2020) and southwestern (Zhang et al., 2009) South China Sea, Bay of Bengal (An et al., 2001) (circles). Blue sites indicates wetter Pliocene conditions and yellow sites indicate drier Pliocene conditions as plotted in Fig. 5. **c**, Regression map of previous DJF SSTs onto PC1. Green circles indicate site locations for the cold tongue SST records mentioned in the text and shown in Fig. 6. The black vectors and black stippled regions in **a**-**c** denote significance at the 90% confidence level. (For interpretation of the colors in the figure(s), the reader is referred to the web version of this article.)

tertropical convergence zone (ITCZ). Numerous studies have linked changes in EASM variability (on millennial to orbital time scales) with displacements in the westerlies (Chiang et al., 2015; Kong et al., 2017; Zhang et al., 2018) and ITCZ (Zhang et al., 2016). On inter-annual timescales, the El Niño Southern Oscillation (ENSO) has also been shown to influence the EASM through atmospheric teleconnections (Wang et al., 2020) (Fig. 1). Establishing the nature of these teleconnections during the Miocene-Pliocene could provide a potential framework with which to explore the links between global climate variability and Asian monsoon dynamics on tectonic time scales. For example, one such pattern that is beginning to emerge from the climate proxy network is an inhomogeneous precipitation pattern across East Asia under varying boundary conditions (Chiang et al., 2015; Kong et al., 2017; Zhang et al., 2018)—the so-called "tripole" pattern that, not unlike the modern climatology, reflects an out-of-phase rainfall expression between northern/southern China and central eastern China. Yet, exploring these patterns on tectonic time scales has posed a major challenge, mainly due to an absence of reliable hydroclimate proxies from sedimentary archives that can be dated with sufficient precision.

To address this data gap, we present a novel terrestrial record of East Asian hydroclimate from organic biomarkers, Glycerol Dialkyl Glycerol Tetraethers (GDGTs), preserved in an eight-million-year long sediment core drilled in the North China Plain (NCP), a region near the northern boundary of the EASM region (Fig. 1). GDGTs are the membrane lipids derived from archaea (*iso*-GDGTs) and bacteria (*br*-GDGTs; See Schouten et al. (2013) for structures), which have been widely used in the studies of palaeo-environmental and palaeo-climatic reconstructions due to their wide distributions in various environments and sensitivity to environmental changes. GDGT-based proxies have been increasingly used to reconstruct the paleo-hydroclimate variations related to the EASM. For example, the abundance ratio of *iso*-GDGTs to *br*-GDGTs, $R_{i/b}$, has been used in a Late Miocene fluvio-lacustrine section to indicate the occurrence of severe drought and alkaline deposits (Xie et al., 2012). The *br*-GDGTs and their methylation and cyclisation proxies MBT(MBT')-CBT have been used to reconstruct soil pH in loess–paleosol sequences on the Chinese Loess Plateau which related to the palaeohydrological conditions (Peterse et al., 2012; Yang et al., 2014). However, iso-GDGTs are usually used for paleoclimate reconstructions in lake environments because the in-situ *br*-GDGTs might affect the applications of indicators (e.g., Tierney and Russell, 2009; Loomis et al., 2011; Buckles et al., 2014). GDGT-0 and Crenarchaeol (abbreviated as Cren) are two widespread *iso*-GDGTs found in aquatic environments. GDGT-0 in lakes and peats are mainly produced by anaerobic archaea like methanogenic Euryarchaeota (Schouten et al., 2000; Pancost et al., 2000; Weijers et al., 2006; Blaga et al., 2009), and are typically more abundant

at shallow depths. Cren is a unique GDGT produced by Thaumarchaeota in the water column and sediments, and has been proposed as an indicator for lake-level changes in both medium and deep lakes (Wang et al., 2014). Therefore, the ratio of GDGT-0 and Cren has the potential to be an indicator of paleo-hydroclimate changes.

The primary goal of this study is to reconstruct the paleo-hydroclimate changes for the past eight million years in the NCP using robust GDGT hydroclimate proxies. To achieve this, we first examined the application of GDGT-0/Cren as a potential new indicator for hydroclimate. We then explore the driving mechanisms to explain the proxy-inferred hydroclimate changes utilizing a suite of novel climate modeling experiments [using the Community Earth System Model (CESM)] forced with "Pliocene-like" boundary conditions.

2. Materials and methods

2.1. Core information and sampling

The G3 drill core (38°49′57.6″N, 117°25′59.5″E) was recovered south of the Hai He River in southeastern Tianjin, NPC. The region's modern mean annual temperature is 12.3 °C (average of −5-3 °C in January, and ∼26 °C in July) with mean annual precipitation (MAP) of ∼520-660 mm. Southeast Tianjin is dominated by the East Asian monsoon system, which contributes to the warm temperate climate of the region.

The G3 drill core is 905 m long and can be divided into six depositional units (Fig. 2). On the bottom layers of the G3 core (e.g. Unit 1), the lithostratigraphy is characterized by several sedimentary cycles composed of medium sands and silt clay, indicating that the sedimentary environments were dominated by fluvial channel/overbank and river floodplains. In the upper layers of the G3 core (from Unit 4 to Unit 2), the sediments are characterized by silt clay and fine sands, showing a dominance of lacustrine and floodplain settings (Yang et al., 2020). The top 60 m of the G3 drill core might occasionally be indicative of marine transgressions resulting in the occurrence of three shelly beds (Fig. 2). Though, a recent provenance study revealed that the sediments were mainly derived from surrounding mountains such as Taihang Mountain and Lvliang Mountains (Yang et al., 2020).

2.2. Age model

The magnetostratigraphic results showed that the pattern of observed paleomagnetic polarity zones can be well correlated to the Late Miocene geo-magnetic polarity time scale (GPTS) (Yang et al., 2020) (Fig. 2). High-resolution magnetostratigraphic results of G3 core assigned an age spanning from ca. 8 Ma to the present, and the Brunhes/Matutama (B/M) and Matuyama/Gauss (M/G) boundaries were at the depth of ∼85 m and ∼240 m, respectively. This well-dated deep drill core allowed us to compare our GDGT-based paleohydrological proxies with other indices.

2.3. Sampling and GDGTs analysis

We collected 119 samples for GDGTs analysis. All samples were stored at −20 °C after being transported to the lab, and later freeze-dried and ground into powder (<60 mesh) with a mortar and pestle. For GDGT analysis, an aliquot of samples (35-55 g) was extracted using an accelerated solvent extractor (ASE) with a mixture of dichloromethane: methanol (DCM: MeOH, 9:1, v/v) at a temperature of 100 °C and pressure of 7.6×10^6 Pa. The combined total lipid extracts (TLE) were rotary evaporated to near dryness at 42 °C. The TLEs were dried under a gentle flow of nitrogen gas and then recovered by extracting with n-hexane, and were then separated into apolar and polar fractions over an Al_2O_3 column using *n*-hexane and DCM: MeOH (1:1, v:v), respectively, as eluents. The polar fraction containing GDGTs was passed through a 0.45 μm PTFE filter and spiked with an aliquot of synthesized internal standard (C_{46} GTGT) for the semi-quantification of GDGT compounds. The polar fraction was then dried under a gentle flow of nitrogen gas. GDGTs were analyzed using an Agilent 1200 series liquid chromatography and triple quadruple mass spectrometry (LC-MS^2) equipped with an autosampler and Masshunter workstation software. GDGTs in all samples were identified using a liquid chromatography and triple quadruple mass spectrometry.

The $R_{i/b}$ index has been used to identify enhanced aridity conditions (Tang et al., 2017; Xie et al., 2012) and calculated as follows:

$$R_{i/b} = \Sigma(iso\text{-GDGTs})/\Sigma(br\text{-GDGTs})$$

GDGT-0/Cren represents the abundance ratio of GDGT-0 to crenarchaeol (Cren).

2.4. Climate model simulations

To investigate the influence of Early Pliocene SSTs on the EASM, two prescribed-SST climate simulations were performed using the Community Earth System Model (CESM) version 1.2.2 with active atmosphere (Community Atmospheric Model, CAM5) and land (CLM4) components ($0.9 \times 1.25°$ resolution) and prescribed SST and sea-ice components. The first simulation is the "preindustrial control" simulation forced with 284.7 ppmv of atmospheric CO_2 concentrations and the default SST and sea-ice cover boundary conditions provided for component set "F_1850_CAM5" which has been derived from the modern HadOISST product. The second simulation is the "Pliocene" simulation forced with an SST field capturing the pattern of large-scale SST change seen in Early Pliocene SST reconstructions. Burls and Fedorov (2014a) presented a fully-coupled (FC) low resolution CESM simulation chosen from a range of modified-cloud-albedo experiments because the pattern of annual-mean SST change (FC Pliocene – FC preindustrial control) matches particularly well with Early Pliocene SST reconstructions. The Pliocene-like SST field from this coupled simulation was then used to force a low-resolution prescribed-SST Pliocene experiment in Burls and Fedorov (2017) in order to isolate and investigate the influence of Pliocene SSTs on the hydrological cycle – with a focus on the arid subtropics. Given the more regional nature of the current study we modify the prescribed-SST approach of Burls and Fedorov (2017) in two main ways: (1) To provide more regional resolution we use a higher resolution configuration of CAM as described above; (2) To remove the influence of global and North Pacific cold biases in the FC preindustrial control (e.g., Burls et al., 2017) on the Pliocene SST field, we force our Pliocene experiment with an SST field derived by adding the 12-month, climatological (Burls and Fedorov, 2014b) FC Pliocene-preindustrial control anomaly field to the HadOISST field used to force our preindustrial control experiment (see Fig. 1 of Burls and Fedorov, 2017 for the annual-mean of this anomaly field and a comparison with the Early Pliocene proxy data). Atmospheric CO_2, aerosols, orography, bathymetry and all other boundary conditions remain the same as the values used within the preindustrial control to isolate the influence of Early Pliocene SSTs on the hydrological cycle.

3. Results and discussion

3.1. Biomarker evidence for Early Pliocene monsoon expansion

GDGT-0 and Cren are the most abundant components among *iso*-GDGTs, with a high dominance of GDGT-0 over Cren in the lower part of the G3 core. Generally speaking, shallow lake surface sediments contain a large amount of GDGT-0, which was likely

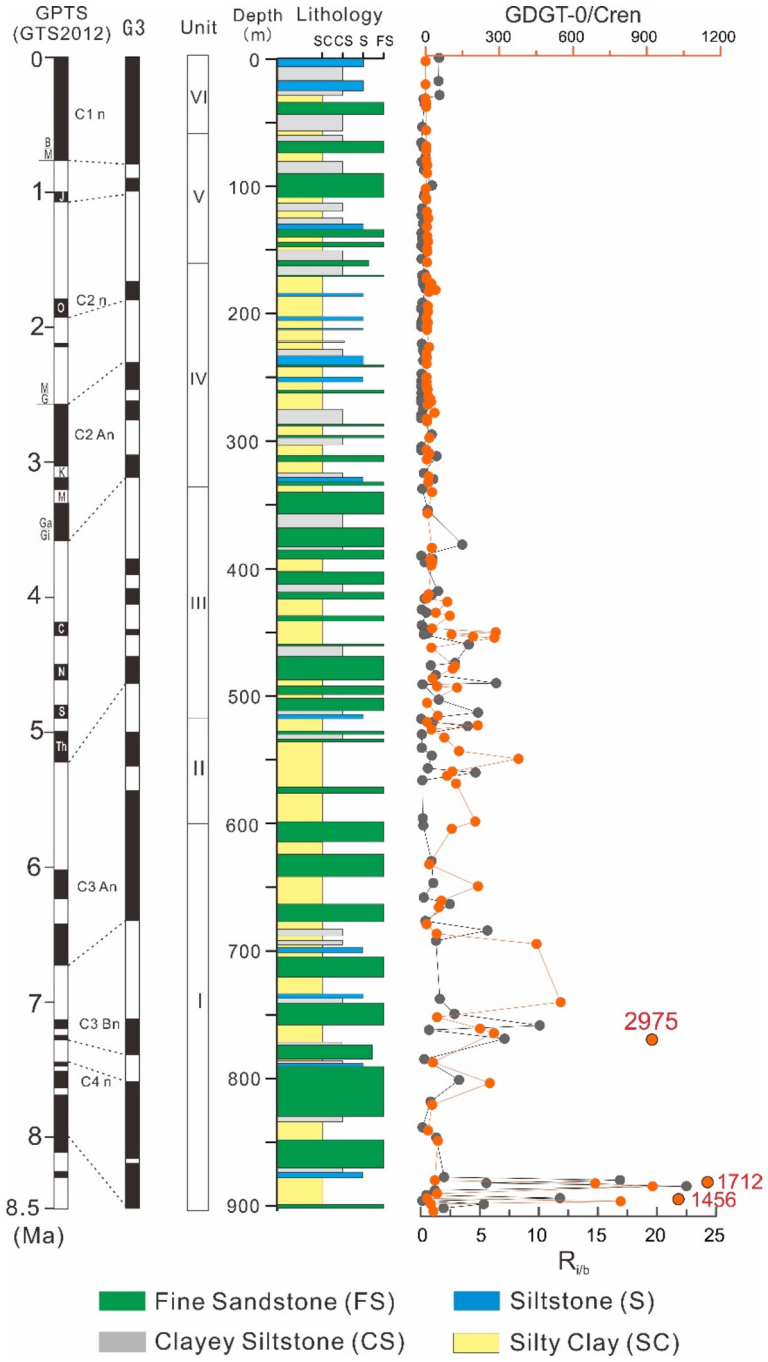

Fig. 2. The variation of GDGT-0/Cren and $R_{i/b}$ in the G3 drill core recovered from the North China Plain. Orange symbols indicate GDGT-0/Cren, gray symbols indicate $R_{i/b}$ values. Lithostratigraphy and magnetostratigraphic results from Yang et al. (2020).

derived from anaerobic archaea, potentially methanogenic archaea (Schouten et al., 2000; Sinninghe Damsté et al., 2002; Blaga et al., 2009). In contrast, Cren is produced specifically by Thaumarchaeota residing in the water column because it needs oxygen for ammonia oxidation. Thus, we propose that the GDGT-0/Cren ratio is a proxy for the contribution of methanogenic Euryarchaeota, with GDGT-0/Cren ratios >2 indicating a substantial loading of methanogenic Euryarchaeota (Blaga et al., 2009). The abundance of Thaumarchaeota have been found to increase with water depth (Tierney et al., 2010; Wang et al., 2014). Based on this empirical relationship between Thaumarchaeota abundance and lake water depth, we calculated the GDGT-0/Cren in modern lake sediments of Qinghai Lake in Northwest China, the largest inland lake in China with a maximum water depth of ca. 30 m, and found a significant negative correlation with the water depth (Fig. 3). Lakes in China are in general medium to small in size and depth, well-mixed, and lack thermal gradients (Dang et al., 2016; Qian et al., 2019). A negative correlation between GDGT-0/Cren in water column SPM and total monthly precipitation was observed in a modern lake study in central China as well (Qian et al., 2019). This is probably due to the significant negative correlation between GDGT-0/Cren and the dissolved oxygen content (DO) in the water column which favored the production of Thaumarchaeota during seasons with higher rainfall (Dang et al., 2016; Qian et al., 2019). Thus, the GDGT-0/Cren is likely to be used as a potential index for hydroclimate in shallow lake environments, with higher values indicating drier conditions.

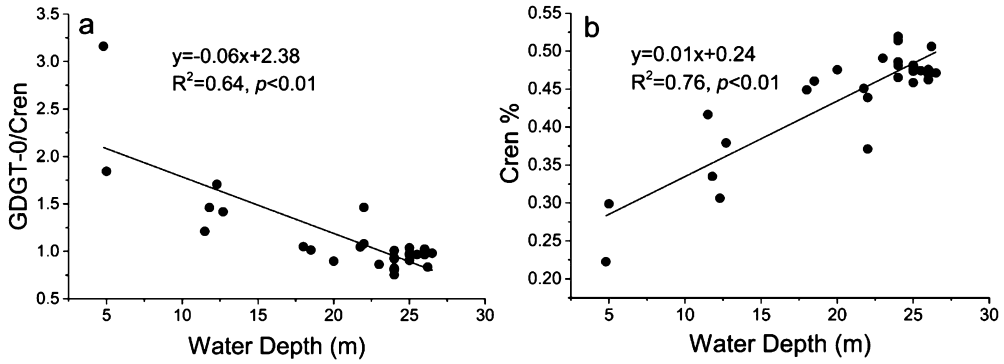

Fig. 3. Correlations of GDGT-0/Cren (a) and abundance of Cren (b) vs. water depth in Qinghai Lake. Data from Wang et al. (2014) and Lu et al., (2016). Data information and sources are listed in Supplemental Table 1.

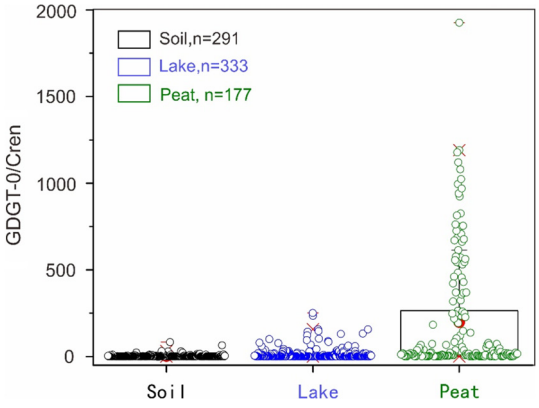

Fig. 4. Box plot of GDGT-0/Cren in modern soils (black), lacustrine sediments (blue) of medium to small sized lakes and peatlands (green) from globally published data. Data information and sources are listed in Supplementary Table 2.

When shallow lakes dry out, turning into peat environments, the abundance of GDGT-0 becomes extremely dominant while the abundance of Cren becomes minimal or undetectable (e.g., Zheng et al., 2015). We further compared data (core lipid fraction) from global modern soils, lacustrine surface sediments of small and medium size lakes (including pond sediments), and peatlands (Supplementary Table 2), and found that GDGT-0/Cren in soils are the lowest while the ratio in peatlands are the highest (i.e. much higher than in lacustrine sediments) (Fig. 4; Data information and sources are listed in Supplementary Information). This indicates that methanogenic archaea are particularly abundant in drier environments (like peat) than lakes and thus the index can be used to indicate the hydrological changes of different sedimentary facies. We therefore interpret a decrease in the GDGT-0/Cren ratio as reflecting increased water depth during wetter periods.

The ratio of GDGT-0/Cren in the G3 core shows distinct difference before and after ~4.5 Ma. From 8 to 4.5 Ma, the GDGT-0/Cren values range from 3.8 to 924.1 (the average value is 148.3), with three extremely high values of 1456.6, 1711.9 and 2975.3 during the period 8 to 7 Ma (Fig. 2). Since ca. 4.5 Ma, GDGT-0/Cren values are consistently low, ranging from 0.3 to 36.5 and average is 9.1. The significant decrease in our GDGT-0/Cren ratio after ~4.2-4.5 Ma (Fig. 2) infers a deep-water depth associated with the relatively wet climate.

Another hydrologic proxy ($R_{i/b}$) that is based on the ratio of *iso*-GDGTs vs. branched GDGTs (*br*-GDGTs) has been increasingly applied to reconstruct paleo-aridity (Tang et al., 2017; Xie et al., 2012). In the G3 core, the *iso*-GDGTs are mainly composed of GDGT-0, and thus the $R_{i/b}$ and the ratio of GDGT-0/Cren are essentially identical. The $R_{i/b}$ index is distinct from alternative hydrologic proxies because it focuses exclusively on moisture rather than both temperature and precipitation, and has been successfully applied to the investigations on paleo-aridity in Neogene fluviolacustrine facies and loess-paleosol sequences (Tang et al., 2017; Xie et al., 2012). The $R_{i/b}$ record in the G3 core also shows distinct difference in the variance and mean state at ~4.2-4.5 Ma, especially, from 8 to 4.2-4.5 Ma values range from 0.9 to 22.5 and average is 2.6, while thereafter values range from 0.02 to 3.5 and average is less than 1. This suggests a critical hydroclimate change from a dry to wet climate state in the NCP during the Early Pliocene.

3.2. Hydroclimatic changes over the East Asia since the Late Miocene

Both hydrological proxies show that the NCP hydroclimate shifted from dry to wet conditions at about 4.2-4.5 Ma ago. Similar shifts are also observed on the Chinese Loess Plateau (CLP) and the South China Sea sedimentary records (Fig. 5). Magnetic susceptibility of a loess-paleosol sequence from the CLP (Lingtai section), a proxy for monsoon rainfall in the semi-arid region of northern China between the summer monsoon domain and the westerlies region, reveals a clear increase in monsoon strength and variability since ~4.2 Ma (Sun et al., 2006), indicating a wetter and more seasonal climate since the Early Pliocene (Fig. 5b). In the monsoon region of the South China Sea (SCS), high-resolution hematite to goethite ratio, an Asian monsoon precipitation proxy from the IODP Site U1431 in central SCS (Gai et al., 2020), and ODP Site 1143 in southwestern SCS (Zhang et al., 2009), both indicate an overall increasing monsoon precipitation trend since the Early Pliocene (Fig. 5e). Interestingly, proxy data also show that the Indian Monsoon experienced a significant increase in strength during the Early Pliocene (An et al., 2001) (Fig. 5f). Together, these records indicate that the Asian paleoclimate transitioned from a relatively dry state to a wetter, monsoon-dominated regime at ~4.2-4.5 Ma.

However, in contrast with the consistent hydrological variations in both northern and southern parts of China and India, the lower reaches of the Yangtze River Valley (YRV) show, in general, an opposing trend since the late Miocene (Fig. 5c, d). Specifically, the ratio of arboreal pollen (AP) to non- arboreal pollen (NAP) of fluvial-lacustrine deposits in the Yangtze River Delta indicates that precipitation in central-eastern China was characterized by a relatively warm and humid climate from the late Miocene to the Early Pliocene, and a cold and dry climate since ~ 4.2 Ma (Zhang et al., 2013). The hydroclimate shifted from wet to dry conditions has also been recorded by smectite/kaolinite records in northern SCS ODP Site 1146, indicative of stronger physical erosion relative to chemical weathering (Wan et al., 2007). Thus, collectively, these data demonstrate a meridional "tripole-like" shift in monsoon rainfall across the region, where the observed dry conditions in northern China and southern Asia, and wet conditions in central-eastern China during the late Miocene completely reverses at around 4.2-4.5 Ma. These findings beg the question of whether a shift in the

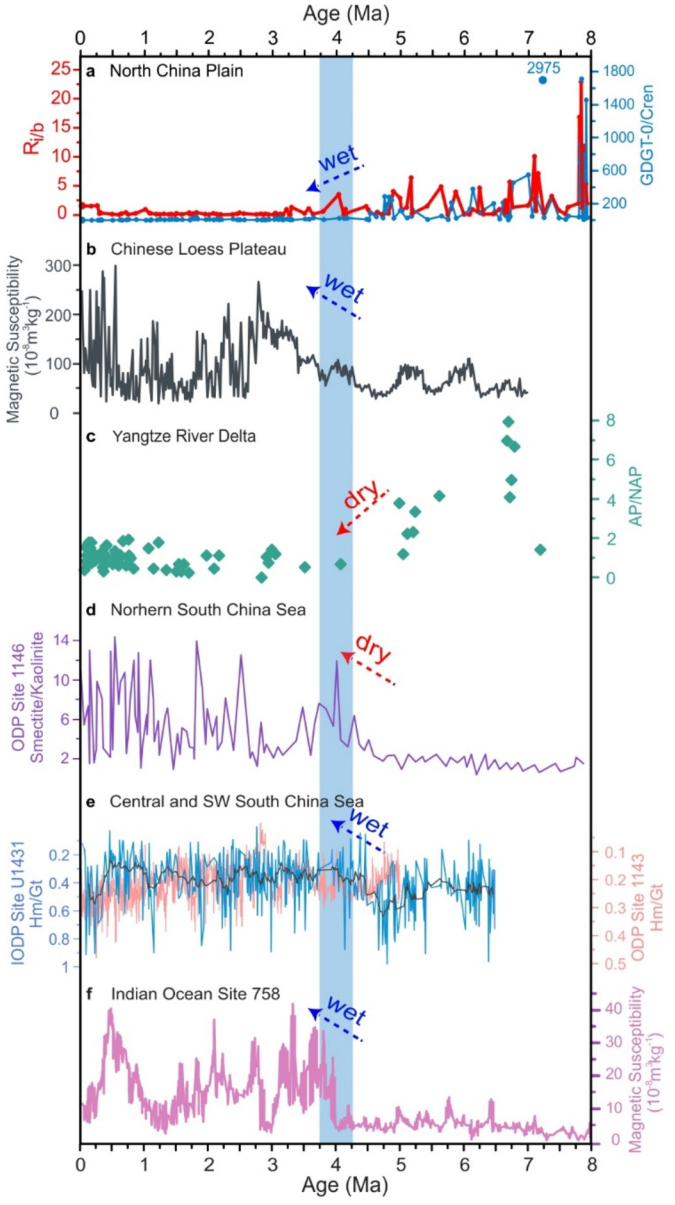

Fig. 5. Hydroclimate tripole pattern across East Asia during the Miocene-Pliocene. **a**, Ratio of GDGT-0/Cren and $R_{i/b}$ proxy in the G3 core from the North China Plain. **b**, Loess magnetic susceptibility data from Chinese Loess Plateau (Sun et al., 2006). **c**, Ratio of arboreal pollen (AP) to non arboreal pollen (NAP) of fluvial-lacustrine core ZK004 in Yangtze River Delta (Zhang et al., 2013). **d**, Smectite/Kaolinite records at ODP Site 1146, northern SCS (Wan et al., 2007). **e**, Hematite/goethite (Hm/Gt) values at IODP Site U1431, central SCS (salmon curve) (Gai et al., 2020) and ODP Site 1143, southwestern SCS (blue curve)(Zhang et al., 2009). **f**, Magnetic susceptibility flux from the Indian Ocean ODP Site 758 (An et al., 2001). Blue vertical bar indicates the significant hydrological changes observed across East Asia at 4.2-4.5 Ma. The black line in **e** is smoothed curve.

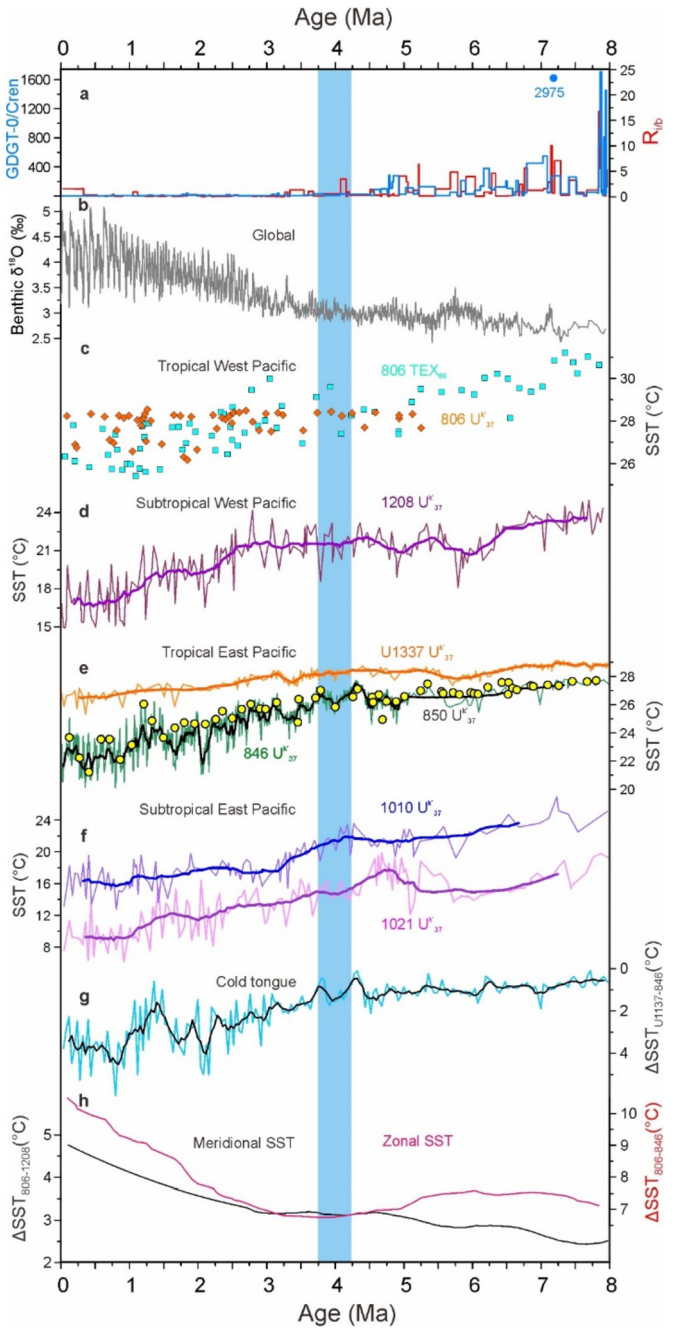

Fig. 6. Temperature evolution of the tropical and midlatitude Pacific since 8 Ma. **a**, GDGT-0/Cren and $R_{i/b}$ records from the NCP. **b**, Global benthic foraminifera $\delta^{18}O$ record (Lisiecki and Raymo, 2005; Zachos et al., 2001). **c**, Records of the tropical West Pacific SST derived from TEX_{86} (cyan square) (Zhang et al., 2014) and $U^{k'}_{37}$ (orange diamond) (Pagani et al., 2010). **d**, $U^{k'}_{37}$-SST of mid-latitude West Pacific (LaRiviere et al., 2012). **e**, Alkenone-derived records tropical East Pacific SST from ODP 846 (green curve) (Herbert et al., 2016; Lawrence et al., 2009), ODP 850 (yellow circle) (Zhang et al., 2014) and U1337 (orange curve) (Liu et al., 2019). **f**, Alkenone-derived mid-latitude East Pacific SST records (LaRiviere et al., 2012): light purple, ODP 1021; blue curve, ODP 1010. **g**, Cold tongue development in the East Pacific (Liu et al., 2019) **h**, Zonal and meridional temperature gradients of the Pacific Ocean since 8 Ma (Zhang et al., 2014). See Fig. 7 for site locations.

tripole pattern could explain the observed changes across East Asia during the Early Pliocene.

3.3. Mechanism for Early Pliocene monsoon changes

Interannual rainfall variability across the region is dominated by the meridional tripole pattern, which is characterized by a zonally elongated and meridionally banded structure, with alternating changes in sign between 20° and 50°N along the East Asian coast (Hsu and Lin, 2007; Zhang et al., 2018; Wang et al., 2020) (Fig. 1 and Figs. S1 and S2). The positive (negative) phase of this pattern is characterized by increased (reduced) rainfall in central-eastern China (i.e. the middle-lower YRV - Huaihe River valleys) and reduced (increased) rainfall in northern and southern China; this has been termed the "−, +, −" meridional tripole pattern. Investigations of interannual and intraseasonal monsoon variability have shown that the EASM is closely tied to the thermal state of the tropical western Pacific and associated convective activity

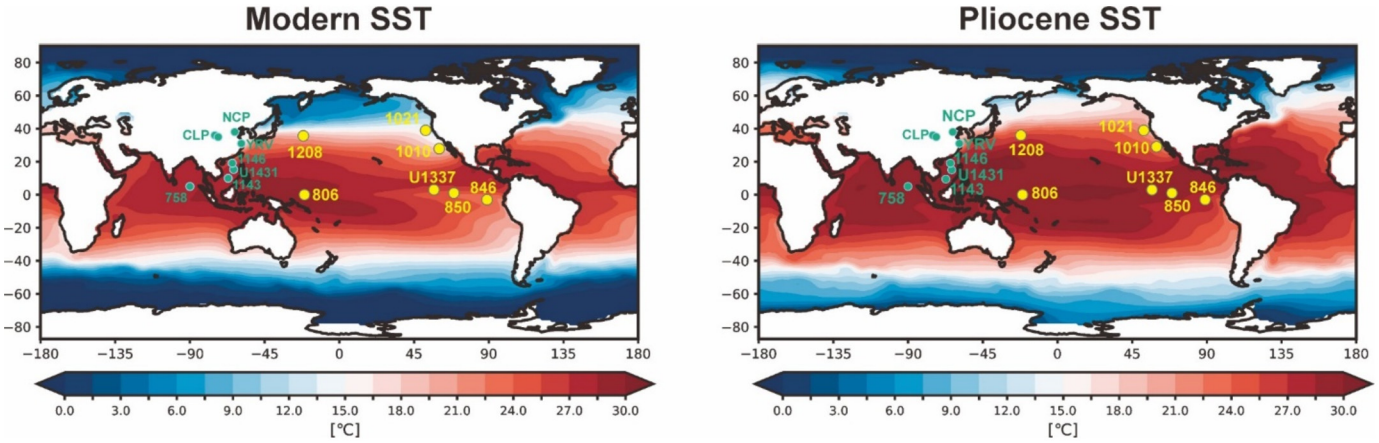

Fig. 7. Modern preindustrial and Pliocene-like SST estimates in our Community Earth System Model (CESM v1.2.2) experiment. SST estimates for the Pliocene simulation were constrained by the marine proxy record. Yellow and green symbols indicate sites of marine SST and East Asian hydroclimate reconstructions, respectively, mentioned in the text and shown in Figs. 5 and 6.

around the Philippines, which controls the northward extension of the EASM system (Huang et al., 2012). When the tropical western Pacific begins warming up during the spring, increased convective activity around the Philippines, along with persistent rainfall in southern China, is followed by a northward shift in the western Pacific subtropical high (WPSH) around mid-June, which marks the onset of the summer monsoon in central eastern China. By mid-July, this monsoon front again jumps northward from the middle-lower YRV - Huaihe River valleys to northeastern China, indicating the commencement of the midsummer stage that is characterized by higher rainfall in the northern latitudes (Fig. S2).

The interannual variability of summer monsoon rainfall anomalies over East Asia have, unsurprisingly, been linked with ENSO, since the tropical SST anomalies are related to the phase of the ENSO mode (Wang et al., 2000; Huang et al., 2012). An empirical orthogonal functional (EOF) analysis of satellite-derived precipitation data for the period 1983-2017 using the Precipitation Estimation from Remotely Sensed Information using Artificial Neural Networks-Climate Data Record (PERSIANN-CDR) reveals that the dominant tripole mode is indeed significantly correlated with eastern Pacific SST anomalies related to ENSO (Wang et al., 2020) (Fig. 1). It has been shown that this ENSO-EASM link derives from the appearance of an anomalous anticyclone over the tropical western Pacific, when lower SSTs in the tropical western Pacific and a weaker Walker circulation occurs shortly after the mature phase of El Niño (Wang et al., 2000, 2003, 2020). Studies have shown that ENSO can also affect the intensity and location of the WPSH. For example, during El Niño events, the WPSH tends to shift to the southwest, while during La Niña events the WPSH retreats northeastward (Zhang et al., 1999; Wang et al., 2003). An additional hypothesis for the ENSO-EASM link relates to a southward shift of the westerly winds impinging on the Tibetan Plateau (Kong and Chiang, 2020); though this mechanism primarily explains early summer (June) rainfall. Whichever mechanism dominates, it is apparent that the positive tripole phase (i.e., wetter central eastern China and drier north/south China) is generally associated with higher eastern equatorial Pacific (EEP) SSTs (i.e. El Niño conditions) and vice versa when EEP SSTs are lower (i.e. La Niña conditions) (Zhang et al., 1999; Hsu and Lin, 2007).

The hypothesis for a "permanent El Niño–like state" (Wara et al., 2005) during the Miocene-Pliocene—i.e., reduced (or absent) mean east–west gradient along the equatorial Pacific—remains controversial (Zhang et al., 2014). Recent data from marine sediment cores have provided compelling evidence for a marked increase in these Pacific zonal and meridional temperature gradients after ca. 4 Ma (Fedorov et al., 2013; LaRiviere et al., 2012; Wycech et al., 2020) (Fig. 6). For example, a recent study found a significant strengthening of the EEP cold tongue at around 4.3 Ma ago (Liu et al., 2019) (Fig. 6g), which the authors attribute to extratropical surface cooling via the "thermocline tunneling mechanism" (Burls and Fedorov, 2014b; Fedorov et al., 2015). In line with previous analyses, the early Pliocene strengthening of the cold tongue occurred in concert with an increasing trend in the meridional SST gradient (Fig. 6h), leading to a strengthening of the Hadley cell and a coincident increase in wind-driven poleward ocean heat transport (Fedorov et al., 2015). It is possible that an increase in the meridional temperature gradient between the tropics and subtropics during the onset of Pliocene cooling at ca. 4 Ma increased the intensity of the Asian monsoon through a strengthening of the Northern Hemisphere (NH) Hadley circulation and the North Pacific high-pressure system. Additionally, the significant correlation between the EASM tripole mode and ENSO in the instrumental record (Fig. 1) offers a modern-day analog of the EASM response to global-scale changes in temperature; in this regard, a reduced Pacific zonal SST gradient and a weaker Walker circulation during the Miocene-Pliocene could have thus inhibited the transport of moisture into northern China as seen in our molecular records.

3.4. Simulated dynamics of Miocene-Pliocene aridity in Northern China

To test the aforementioned hypotheses that the weaker Early Pliocene meridional and zonal SST gradients maintained the positive tripole-mode-like conditions suggested by the data prior to ~4.3 Ma, we analyzed an atmospheric climate model simulation that was driven by SSTs that closely resemble Early Pliocene palaeoceanographic reconstructions (Burls and Fedorov, 2017) (Fig. 7); refer to Methods and references contained in Fedorov et al. (2015) and Burls and Fedorov (2014b) for a detailed description of the coupled Pliocene simulation from which the Early Pliocene SST anomaly was derived. Our Pliocene-like model results are in general agreement with the proxy records from East Asia, showing overall drier summer monsoon conditions in northern China, the central and southwestern South China Sea, and the Bay of Bengal, but wetter monsoon conditions in central eastern China and northern SCS (Fig. 8a). To investigate the dynamical mechanisms that explain these changes, we first examine the Pliocene shifts in the monsoon through the lens of a recent hypothesis—the "Jet Transition Hypothesis" (JTH) (Chiang et al., 2015); the JTH proposes that changes in the meridional position of the westerlies relative to the Tibetan Plateau can influence the intraseasonal stages of EASM evolution (i.e., spring, pre-Meiyu, Meiyu, and midsummer), whereby an earlier end to the Meiyu stage lengthens

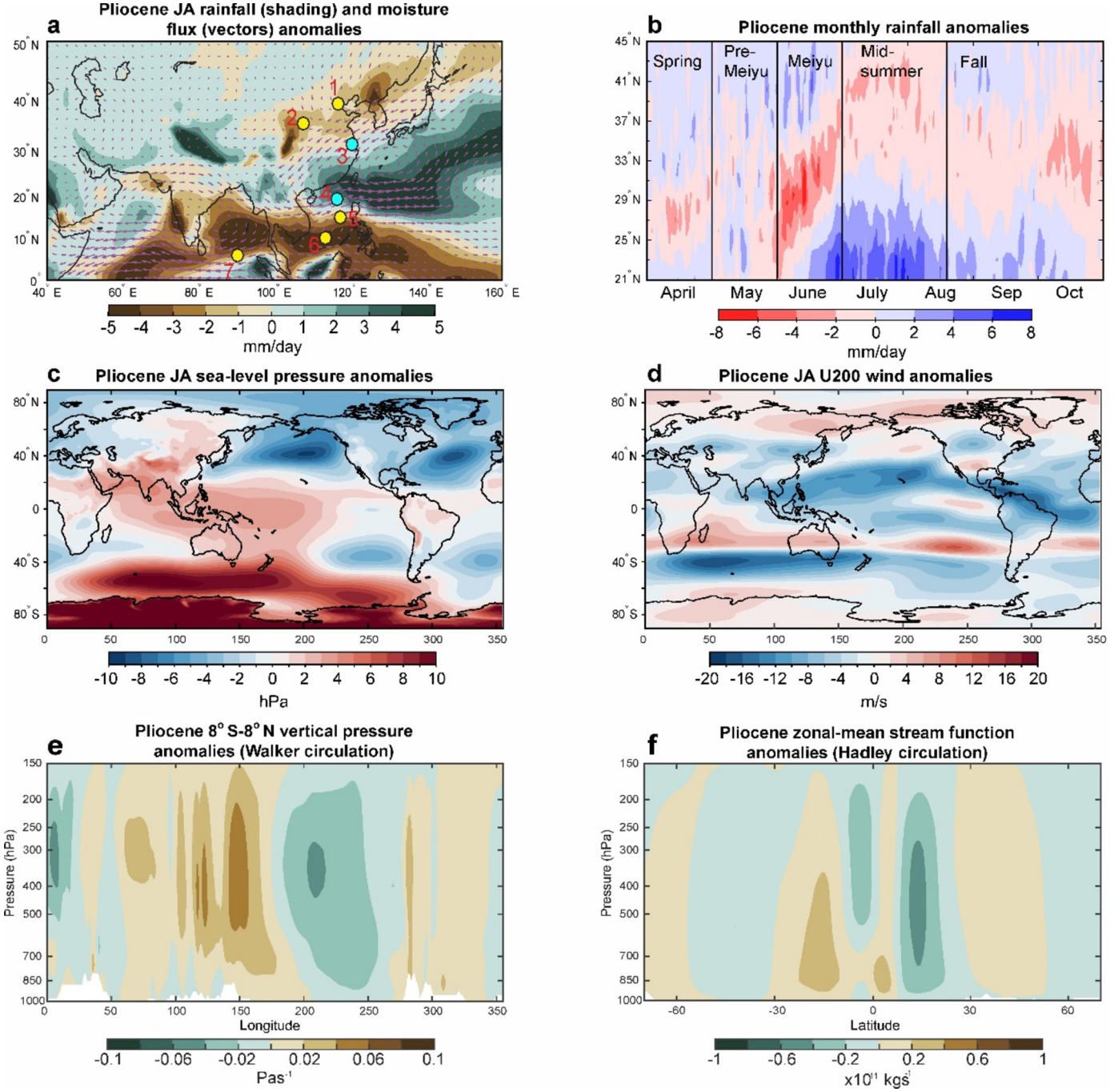

Fig. 8. Atmospheric circulation anomalies for the Pliocene minus preindustrial control run climate model simulations. a, July-August (JA) rainfall (shading) and moisture flux (vectors). Black symbols indicate the various study sites mentioned in the text (sites 1: North China Plain, this study; 2: Chinese Loess Plateau; 3, the lower reaches of the Yangtze River Valley; 4, the northern South China Sea; 5, central South China Sea; 6, the southwestern South China Sea; 7, Bay of Bengal). **b**, Hovmöller diagram of precipitation anomalies over eastern China (110° to 125°E). Approximate timings of the various intraseasonal stages are shown. **c**, JA sea-level pressure and **d**, 200 hPa zonal wind anomalies. **e**, JA vertical pressure velocity anomalies along the equator (computed as deviations from zonal mean and averaged between 8° S and 8° N) and **f**, zonal mean stream function. Brown (green) colors in **e** indicate anomalous downward (upward) flow, while brown (green) colors in **f** indicate counterclockwise (clockwise) flow.

the midsummer stage, resulting in more rainfall in northeastern China but less rainfall over central eastern China. This mechanism, which primarily derives from shifts in equator-to-pole temperature gradients, has been shown to have operated on a range of time scales, including current and future interannual variability (Chiang et al., 2017, 2019), orbital-scale changes through the Holocene (Kong et al., 2017), and millennial-scale shifts during Termination I (Zhang et al., 2018). Close inspection of our model results, however, show no obvious difference in the timing of monsoon onset in northeastern China between the Pliocene and preindustrial control runs (Fig. S3), rather a magnitude change, particularly during the midsummer stage (Fig. 8b) which shows much lower rainfall in the Pliocene simulation. Therefore, the JTH does not appear to be the primary mechanism behind the simulated East Asian rainfall changes during the Early Pliocene. In addition, given the critical connection between the JTH and the Tibetan Plateau (Chiang et al., 2015), it is thus unlikely that the uplift of the Plateau around 3.6 Ma (An et al., 2001), occurring mainly in the northeastern Plateau (Li et al., 2017), can explain the northward shift in monsoon rainfall during the Early Pliocene. However, we cannot

rule out the possibility that an uplifted Plateau helped maintain the northward extension of the monsoon through the Pliocene-Pleistocene given previous modeling experiments (e.g., Chen and Bordoni, 2016) showing a strong influence of the Tibetan Plateau on the EASM.

Alternatively, the tripole-like shift may stem from the influence of Pacific SST gradients (Fig. 7) on the Walker circulation and convection in the WPWP region (Fig. 8). As previously noted, modern-day interannual tropical Pacific and Indian Ocean SST variability (related to ENSO) has a strong influence on the EASM (Hsu and Lin, 2007; Wang et al., 2000; Wu et al., 2003; Wang et al., 2020), and particularly the dominant tripole mode (Fig. 1). During El Niño years, anomalously high pressure in the western Pacific, along with stronger southeasterly winds along the western margin of this anticyclone, can act to increase precipitation in central eastern China (Wang et al., 2000; Wu et al., 2003; Wang et al., 2020). In addition, the tripole pattern has also been tied to tropical western Pacific SSTs and convection around the Philippines via the so-called "Pacific-Japan (PJ) pattern" or the "East Asia/Pacific (EAP) pattern" (Huang et al., 2012; Kosaka and Nakamura, 2010), shown to be a dominant mode of atmospheric circulation anomalies over East Asia during boreal summer (Lu et al., 2006). The PJ pattern, which typically follows warmer tropical central/eastern Pacific SST anomalies, is characterized by higher rainfall in the YRV and Huaihe Rivers, but droughts in northern China (Hsu and Lin, 2007; Huang et al., 2012). Synoptic-scale precursors of the PJ pattern with extreme rainfall in the YRV show that the associated tripole configuration of rainfall is modulated by a strong anticyclone-cyclone pair in the midlatitudes of East Asia (Chen and Zhai, 2015). This pattern is evident in our Pliocene-like simulations, which show a steeper Pliocene pressure gradient over East Asia due to higher sea-level pressure (SLP) in the South China Sea and Philippines Sea, and lower SLP in the East China Sea (Fig. 8c). The resulting confluence between the northerly winds, directed by the anomalous cyclonic flow, and the southwesterly winds, directed around the anticyclonic flow, would have promoted atmospheric convergence in the YRV region (Fig. 8a). Our results are in line with recent model and observational analyses of the effects of ENSO and equatorial warming on the EASM. For example, Kong and Chiang (2020) recently demonstrated that years following El Niño events are characterized by increased early summer monsoon rainfall in East Asia due to an enhancement of the extratropical northerlies downstream of the TP (due to tropospheric warming-induced strengthening of the subtropical jet impinging on the TP), which promotes convergence in central-eastern China. Our findings (Fig. 8) are also consistent with future projections of the EASM under the high emissions RCP8.5 scenario (e.g. Chiang et al., 2019; Zhou et al., 2019), which show that increased equatorial warming, akin to conditions of the Pliocene, causes a regional equatorward contraction of the subtropical circulation and thus a southward shift of the subtropical jet and Meiyu-Baiu rainband.

Our findings suggesting a strong connection between SST gradients and atmospheric circulation, in particular the overall weaker Hadley and Walker circulations, are also consistent with recent studies of Pliocene hydroclimate. For example, Burls and Fedorov (2017) recently demonstrated, using a modeling framework similar to that of this study, that weaker zonal and meridional temperature gradients during the Pliocene led to reduced subtropical moisture divergence, a finding consistent with our simulations (Figs. 8e and 8f; Figs. S4 and S5). A greatly expanded WPWP, combined with a significant reduction in the southwesterly monsoon flow over East Asia (Figs. 8a and 8d), would have also translated to a reduction in the northward transport of monsoonal moisture, while increased convergence in the SCS would have led to much higher rainfall in central-eastern China. There is support for this from the instrumental record, which has shown that a weaker Asian monsoon circulation can lead to increased drought frequency in northern China due to a reduction in the transport of water vapor to the higher latitudes (e.g., Zhang and Zhou, 2015).

4. Conclusions

Our new hydrological record based on the microbial ratio of GDGT-0/Cren and $R_{i/b}$ index shows a significant strengthening of the EASM in the NCP during the Early Pliocene, around ~4.2-4.5 Ma, in concert with the development of the EEP cold tongue. From our analysis of modern instrumental data and Pliocene-like climate model simulations, we posit that the large-scale changes in both zonal and meridional temperature gradients strengthened both the Walker and Hadley circulations respectively. As a result, strengthening in atmospheric circulation along with a shift in western Pacific convective processes likely facilitated an increase in meridional moisture flux to northern China, at the expense of central eastern China when SST gradients increased during the Early Pliocene. Our findings provide critical new insight into the sensitivity and heterogeneity of the EASM system response to basin-wide changes in meridional and zonal temperature gradients, and thus provide an important new paleo perspective for future projections of the EASM under global warming. Our study supports recent modeling efforts which suggest a contraction of the EASM in response to future equatorial warming, posing future challenges to the populated regions of both southern and northern China.

CRediT authorship contribution statement

Jiayi Lu: Data curation, Investigation, Writing – original draft. **Huan Yang:** Investigation, Resources, Writing – review & editing. **Michael L. Griffiths:** Methodology, Project administration, Writing – original draft. **Natalie J. Burls:** Investigation, Methodology, Writing – review & editing. **Guoqiao Xiao:** Resources. **Jilong Yang:** Data curation, Resources. **Jessica K. Wang:** Resources, Writing – review & editing. **Kathleen R. Johnson:** Writing – review & editing. **Shucheng Xie:** Conceptualization, Funding acquisition, Supervision, Writing – review & editing.

Data availability

The data supporting the findings of this study are available within the paper and its Supplementary Information files.

Declaration of competing interest

The authors declare that they have no known competing financial interests or personal relationships that could have appeared to influence the work reported in this paper.

Acknowledgements

We thank Shi Qian and Cheng Weng for their assistance with sampling and experiments. We thank Dr. Yige Zhang, Hongbin Zhang, Qiuying Zhang and Xinyue Dang for their constructive discussions. We thank Dr. Yemane Asmerom for his editorial handling and two anonymous reviewers for their thoughtful reviews. The work was sponsored by National Natural Science Foundation of China (Grant No. 41830319, 41821001, 41972196), the State Key R&D Program of China (Grant No. 2016YFA0601100) and 111 Project (Grant No. BP0820004). Natalie J. Burls acknowledges support from the National Science Foundation (NSF; AGS-1844380 and OCN-2002448), as well as the Alfred P. Sloan Foundation as a Research Fellow.

Appendix A. Supplementary material

Supplementary material related to this article can be found online at https://doi.org/10.1016/j.epsl.2021.116882.

References

An, Z., Kutzbach, John E., Prell, Warren L., Porter, Stephen C., 2001. Evolution of Asian monsoons and phased uplift of the Himalaya–Tibetan Plateau since Late Miocene times. Nature 411, 62–66.

An, Z., Sun, Y., Chang, H., Zhang, P., Liu, X., Cai, Y., Jin, Z., Qiang, X., Zhou, W., Li, L., Shi, Z., Tan, L., Li, X., Zhang, X., Jin, Z., 2014. Late Cenozoic Climate Change in Monsoon-Arid Asia and Global Changes, vol. 16, pp. 491–581.

Ashouri, H., Hsu, K.L., Sorooshian, S., Braithwaite, D.K., Knapp, K.R., Cecil, L.D., Nelson, B.R., Prat, O.P., 2015. PERSIANN-CDR: daily precipitation climate data record from multisatellite observations for hydrological and climate studies. Bull. Am. Meteorol. Soc. 96 (1), 69–83.

Blaga, C.I., Reichart, G.-J., Heiri, O., Damsté, J.S.S., 2009. Tetraether membrane lipid distributions in water-column particulate matter and sediments: a study of 47 European lakes along a North–South transect. J. Paleolimnol. 41, 523–540.

Buckles, L.K., Weijers, J.W., Verschuren, D., Damsté, J.S.S., 2014. Sources of core and intact branched tetraether membrane lipids in the lacustrine environment: anatomy of Lake Challa and its catchment, equatorial East Africa. Geochim. Cosmochim. Acta 140, 106–126.

Burls, N., Fedorov, A., 2014a. Simulating Pliocene warmth and a permanent El Niño-like state: the role of cloud albedo. Paleoceanography 29, 893–910.

Burls, N., Fedorov, A., 2014b. What controls the mean East–West sea surface temperature gradient in the equatorial Pacific: the role of cloud albedo. J. Climate 27, 2757–2778.

Burls, N.J., Fedorov, A.V., 2017. Wetter subtropics in a warmer world: contrasting past and future hydrological cycles. Proc. Natl. Acad. Sci. 114, 12888–12893.

Burls, N.J., Muir, L., Vincent, E.M., Fedorov, A., 2017. Extra-tropical origin of equatorial Pacific cold bias in climate models with links to cloud albedo. Clim. Dyn. 49, 2093–2113.

Chen, J., Bordoni, S., 2016. Early summer response of the East Asian summer monsoon to atmospheric CO2 forcing and subsequent sea surface warming. J. Climate 29, 5431–5446.

Chen, Y., Zhai, P., 2015. Synoptic-scale precursors of the East Asia/Pacific teleconnection pattern responsible for persistent extreme precipitation in the Yangtze River Valley. Q. J. R. Meteorol. Soc. 141, 1389–1403.

Chiang, J.C., Fung, I.Y., Wu, C.-H., Cai, Y., Edman, J.P., Liu, Y., Day, J.A., Bhattacharya, T., Mondal, Y., Labrousse, C.A., 2015. Role of seasonal transitions and westerly jets in East Asian paleoclimate. Quat. Sci. Rev. 108, 111–129.

Chiang, J.C.H., Swenson, L.M., Kong, W., 2017. Role of seasonal transitions and the westerlies in the interannual variability of the East Asian summer monsoon precipitation. Geophys. Res. Lett. 44, 3788–3795.

Chiang, J.C., Fischer, J., Kong, W., Herman, M.J., 2019. Intensification of the pre-Meiyu rainband in the late 21st century. Geophys. Res. Lett. 46 (13), 7536–7545.

Dang, X., Xue, J., Yang, H., Xie, S., 2016. Environmental impacts on the distribution of microbial tetraether lipids in Chinese lakes with contrasting pH: implications for lacustrine paleoenvironmental reconstructions. Sci. China Earth Sci. 59, 939–950.

Fedorov, A.V., Brierley, C.M., Lawrence, K.T., Liu, Z., Dekens, P.S., Ravelo, A.C., 2013. Patterns and mechanisms of early Pliocene warmth. Nature 496, 43–49.

Fedorov, A.V., Burls, N.J., Lawrence, K.T., Peterson, L.C., 2015. Tightly linked zonal and meridional sea surface temperature gradients over the past five million years. Nat. Geosci. 8, 975–980.

Gai, C., Liu, Q., Roberts, A.P., Chou, Y., Zhao, X., Jiang, Z., Liu, J., 2020. East Asian monsoon evolution since the Late Miocene from the South China Sea. Earth Planet. Sci. Lett. 530, 115960.

Guo, Z., 2004. Late Miocene–Pliocene development of Asian aridification as recorded in the red-Earth formation in northern China. Glob. Planet. Change 41, 135–145.

Herbert, T., Lawrence, K., Tzanova, A., Peterson, L., Caballero Gill, R., Kelly, C., 2016. Late Miocene global cooling and the rise of modern ecosystems. Nat. Geosci. 9, 843–847.

Hsu, H.-H., Lin, S.-M., 2007. Asymmetry of the tripole rainfall pattern during the East Asian summer. J. Climate 20, 4443–4458.

Huang, R., Chen, J., Wang, L., Lin, Z., 2012. Characteristics, processes, and causes of the spatio-temporal variabilities of the East Asian monsoon system. Adv. Atmos. Sci. 29, 910–942.

Kong, W., Swenson, L.M., Chiang, J.C., 2017. Seasonal transitions and the westerly jet in the Holocene East Asian summer monsoon. J. Climate 30, 3343–3365.

Kong, W., Chiang, J.C., 2020. Southward shift of westerlies intensifies the East Asian early summer rainband following El Niño. Geophys. Res. Lett. 47 (17), e2020GL088631.

Kosaka, Y., Nakamura, H., 2010. Mechanisms of meridional teleconnection observed between a summer monsoon system and a subtropical anticyclone. Part I: the Pacific–Japan pattern. J. Climate 23, 5085–5108.

LaRiviere, J.P., Ravelo, A.C., Crimmins, A., Dekens, P.S., Ford, H.L., Lyle, M., Wara, M.W., 2012. Late Miocene decoupling of oceanic warmth and atmospheric carbon dioxide forcing. Nature 486, 97–100.

Lawrence, K.T., Herbert, T.D., Brown, C.M., Raymo, M.E., Haywood, A.M., 2009. High-amplitude variations in North Atlantic sea surface temperature during the early Pliocene warm period. Paleoceanography 24, PA2218.

Li, J., Fang, X., Song, C., Pan, B., Ma, Y., Yan, M., 2017. Late Miocene–quaternary rapid stepwise uplift of the NE Tibetan Plateau and its effects on climatic and environmental changes. Quat. Res. 81, 400–423.

Lisiecki, L.E., Raymo, M.E., 2005. A Pliocene-Pleistocene stack of 57 globally distributed benthic δ18O records. Paleoceanography 20, PA1003.

Liu, J., Tian, J., Liu, Z., Herbert, T.D., Fedorov, A.V., Lyle, M., 2019. Eastern equatorial Pacific cold tongue evolution since the late Miocene linked to extratropical climate. Sci. Adv. 5, eaau6060.

Loomis, S.E., Russell, J.M., Damsté, J.S.S., 2011. Distributions of branched GDGTs in soils and lake sediments from western Uganda: implications for a lacustrine paleothermometer. Org. Geochem. 42, 739–751.

Lu, J., Yang, H., Zheng, F., Dang, X., Li, Y., Xie, S., 2016. Contrasting distributions of bacterial branched tetraethers along a soil-river-lake transect in the arid region of Northwestern China. Geochem. J. 50, 249–265.

Lu, R., Li, Y., Dong, B., 2006. External and internal summer atmospheric variability in the western North Pacific and East Asia. J. Meteorol. Soc. Jpn., Ser. II 84, 447–462.

Pagani, M., Liu, Z., LaRiviere, J., Ravelo, A.C., 2010. High Earth-system climate sensitivity determined from Pliocene carbon dioxide concentrations. Nat. Geosci. 3, 27–30.

Pancost, R.D., Damsté, J.S.S., de Lint, S., van der Maarel, M.J., Gottschal, J.C., 2000. Biomarker evidence for widespread anaerobic methane oxidation in Mediterranean sediments by a consortium of methanogenic archaea and bacteria. Appl. Environ. Microbiol. 66, 1126–1132.

Peterse, F., van der Meer, J., Schouten, S., Weijers, J.W., Fierer, N., Jackson, R.B., Kim, J.-H., Damsté, J.S.S., 2012. Revised calibration of the MBT–CBT paleotemperature proxy based on branched tetraether membrane lipids in surface soils. Geochim. Cosmochim. Acta 96, 215–229.

Qian, S., Yang, H., Dong, C., Wang, Y., Wu, J., Pei, H., Dang, X., Lu, J., Zhao, S., Xie, S., 2019. Rapid response of fossil tetraether lipids in lake sediments to seasonal environmental variables in a shallow lake in central China: implications for the use of tetraether-based proxies. Org. Geochem. 128, 108–121.

Schouten, S., Hopmans, E.C., Damsté, J.S.S., 2013. The organic geochemistry of glycerol dialkyl glycerol tetraether lipids: a review. Org. Geochem. 54, 19–61.

Schouten, S., Hopmans, E.C., Pancost, R.D., Damsté, J.S.S., 2000. Widespread occurrence of structurally diverse tetraether membrane lipids: evidence for the ubiquitous presence of low-temperature relatives of hyperthermophiles. Proc. Natl. Acad. Sci. 97, 14421–14426.

Sinninghe Damsté, J.S., Schouten, S., Hopmans, E.C., van Duin, A.C., Geenevasen, J.A., 2002. Crenarchaeol the characteristic core glycerol dibiphytanyl glycerol tetraether membrane lipid of cosmopolitan pelagic crenarchaeota. J. Lipid Res. 43, 1641–1651.

Sun, Y., Lu, H., An, Z., 2006. Grain size of loess, palaeosol and red clay deposits on the Chinese Loess Plateau: significance for understanding pedogenic alteration and palaeomonsoon evolution. Palaeogeogr. Palaeoclimatol. Palaeoecol. 241, 129–138.

Tang, C., Yang, H., Pancost, R.D., Griffiths, M.L., Xiao, G., Dang, X., Xie, S., 2017. Tropical and high latitude forcing of enhanced megadroughts in Northern China during the last four terminations. Earth Planet. Sci. Lett. 479, 98–107.

Tierney, J.E., Russell, J.M., 2009. Distributions of branched GDGTs in a tropical lake system: implications for lacustrine application of the MBT/CBT paleoproxy. Org. Geochem. 40, 1032–1036.

Tierney, J.E., Russell, J.M., Eggermont, H., Hopmans, E., Verschuren, D., Damsté, J.S., 2010. Environmental controls on branched tetraether lipid distributions in tropical East African lake sediments. Geochim. Cosmochim. Acta 74, 4902–4918.

Wan, S., Li, A., Clift, P.D., Stuut, J.-B.W., 2007. Development of the East Asian monsoon: mineralogical and sedimentologic records in the northern South China Sea since 20 Ma. Palaeogeogr. Palaeoclimatol. Palaeoecol. 254, 561–582.

Wang, B., Wu, R., Fu, X., 2000. Pacific–East Asian teleconnection: how does ENSO affect East Asian climate? J. Climate 13, 1517–1536.

Wang, B., Wu, R., Li, T., 2003. Atmosphere–warm ocean interaction and its impacts on Asian–Australian monsoon variation. J. Climate 16, 1195–1211.

Wang, H., Dong, H., Zhang, C.L., Jiang, H., Zhao, M., Liu, Z., Lai, Z., Liu, W., 2014. Water depth affecting thaumarchaeol production in Lake Qinghai, northeastern Qinghai–Tibetan Plateau: implications for paleo lake levels and paleoclimate. Chem. Geol. 368, 76–84.

Wang, H., Lu, H., Zhao, L., Zhang, H., Lei, F., Wang, Y., 2019. Asian monsoon rainfall variation during the Pliocene forced by global temperature change. Nat. Commun. 10, 5272.

Wang, J.K., Yu, J.-Y., Johnson, K.R., 2020. Pacific and Atlantic controls of the relationship between Mainland Southeast Asia and East China interannual precipitation variability. Clim. Dyn. 54, 4279–4292.

Wara, M.W., Ravelo, A.C., Delaney, M.L., 2005. Permanent El Niño-like conditions during the Pliocene warm period. Science 309, 758–761.

Weijers, J.W., Schouten, S., Spaargaren, O.C., Damsté, J.S.S., 2006. Occurrence and distribution of tetraether membrane lipids in soils: implications for the use of the TEX86 proxy and the BIT index. Org. Geochem. 37, 1680–1693.

Wu, R., Hu, Z.-Z., Kirtman, B.P., 2003. Evolution of ENSO-related rainfall anomalies in East Asia. J. Climate 16, 3742–3758.
Wycech, J., Gill, E., Rajagopalan, B., Marchitto Jr, T., Molnar, P., 2020. Multiproxy reduced-dimension reconstruction of Pliocene equatorial Pacific sea surface temperatures. Paleoceanogr. Paleoclimatol. 35 (1), e2019PA003685.
Xie, S., Pancost, R.D., Chen, L., Evershed, R.P., Yang, H., Zhang, K., Huang, J., Xu, Y., 2012. Microbial lipid records of highly alkaline deposits and enhanced aridity associated with significant uplift of the Tibetan Plateau in the Late Miocene. Geology 40, 291–294.
Yang, H., Pancost, R.D., Dang, X., Zhou, X., Evershed, R.P., Xiao, G., Tang, C., Gao, L., Guo, Z., Xie, S., 2014. Correlations between microbial tetraether lipids and environmental variables in Chinese soils: optimizing the paleo-reconstructions in semi-arid and arid regions. Geochim. Cosmochim. Acta 126, 49–69.
Yang, J., Liang, M., Algeo, T.J., Xu, Q., Hu, Y., Yuan, H., Xiao, G., 2020. Upper Miocene-quaternary magnetostratigraphy and magnetic susceptibility from the Bohai Bay Basin (eastern China) and implications for regional volcanic and basinal subsidence history. Palaeogeogr. Palaeoclimatol. Palaeoecol. 538, 109469.
Zachos, J., Pagani, M., Sloan, L., Thomas, E., Billups, K., 2001. Trends, rhythms, and aberrations in global climate 65 Ma to present. Science 292, 686–693.
Zhang, H., Griffiths, M.L., Chiang, J.C., Kong, W., Wu, S., Atwood, A., Huang, J., Cheng, H., Ning, Y., Xie, S., 2018. East Asian hydroclimate modulated by the position of the westerlies during termination I. Science 362, 580–583.
Zhang, H., Griffiths, M.L., Huang, J., Cai, Y., Wang, C., Zhang, F., Cheng, H., Ning, Y., Hu, C., Xie, S., 2016. Antarctic link with East Asian summer monsoon variability during the Heinrich Stadial–Bølling interstadial transition. Earth Planet. Sci. Lett. 453, 243–251.
Zhang, L., Zhou, T., 2015. Drought over East Asia: a review. J. Climate 28, 3375–3399.
Zhang, P., Miao, Y., Zhang, Z., Lu, S., Zhang, Y., Chen, H., Li, X., Miao, Q., Feng, W., Ou, J., Gong, X., Jiang, B., Li, W., 2013. Late Cenozoic sporopollen records in the Yangtze River Delta, East China and implications for East Asian summer monsoon evolution. Palaeogeogr. Palaeoclimatol. Palaeoecol. 388, 153–165.
Zhang, R., Sumi, A., Kimoto, M., 1999. A diagnostic study of the impact of El Nino on the precipitation in China. Adv. Atmos. Sci. 16, 229–241.
Zhang, Y.G., Ji, J., Balsam, W., Liu, L., Chen, J., 2009. Mid-Pliocene Asian monsoon intensification and the onset of Northern Hemisphere glaciation. Geology 37, 599–602.
Zhang, Y.G., Pagani, M., Liu, Z., 2014. A 12-million-year temperature history of the tropical Pacific Ocean. Science 344, 84–87.
Zheng, Y., Li, Q., Wang, Z., Naafs, B.D.A., Yu, X., Pancost, R.D., 2015. Peatland GDGT records of Holocene climatic and biogeochemical responses to the Asian Monsoon. Org. Geochem. 87, 86–95.
Zhou, W., Xie, S.P., Yang, D., 2019. Enhanced equatorial warming causes deep-tropical contraction and subtropical monsoon shift. Nat. Clim. Change 9 (11), 834–839.